

Mixed-Integer Optimal Control via Reinforcement Learning: A Case Study on Hybrid Vehicle Energy Management

Jinming Xu and Yuan Lin, *Member, IEEE*

Abstract—Many optimal control problems require the simultaneous output of continuous and discrete control variables. Such problems are usually formulated as mixed-integer optimal control (MIOC) problems, which are challenging to solve due to the complexity of the solution space. Numerical methods such as branch-and-bound are computationally expensive and unsuitable for real-time control. This brief proposes a novel continuous-discrete reinforcement learning (CDRL) algorithm, twin delayed deep deterministic actor-Q (TD3AQ), for MIOC problems. TD3AQ combines the advantages of both actor-critic and Q-learning methods, and can handle the continuous and discrete action spaces simultaneously. The proposed algorithm is evaluated on a plug-in hybrid electric vehicle (PHEV) energy management problem, where real-time control of the continuous variable, engine torque, and discrete variables, gear shift and clutch engagement/disengagement, is essential to maximize fuel economy while satisfying driving constraints. Simulation results on different drive cycles show that TD3AQ achieves near-optimal control compared to dynamic programming (DP) and outperforms baseline reinforcement learning algorithms.

Index Terms—Mixed-integer optimal control, reinforcement learning, hybrid action space, hybrid electric vehicle energy management.

I. INTRODUCTION

MIXED-INTEGER optimal control (MIOC) problems commonly arise in various engineering applications, such as assignment problems [1], control of piecewise-affine (PWA) systems [2] and hybrid systems [3]. These problems are particularly challenging as they require optimization of a system that involves both continuous and discrete control variables.

One common approach for solving MIOC problems is to formulate them as mixed-integer programming (MIP) models and apply the branch-and-bound method [4]. This method involves dividing the solution space into smaller branches and using a bounding function to determine if each branch can be eliminated. Although it can provide globally optimal solutions, it is computationally expensive and time-consuming. Another approach is to use dynamic programming (DP), which breaks the problem into smaller sub-problems and solves them recursively [5]. However, DP requires discretization of

continuous variables and knowledge of the entire state space in advance, making it less suitable for real-world optimal control. Heuristic algorithms offer feasible and fast solutions by leveraging problem-specific knowledge to guide the search [6], [7], but they may not provide optimality guarantees and require customization for each problem structure [7].

The development of reinforcement learning (RL) has led to a new paradigm for solving complex control problems [8], [9]. RL learns a policy that maps the current state of the system to an action that maximizes the expected cumulative reward. With the learned policy, RL can reach a near-optimal solution without requiring any prior knowledge of the environment [10]. However, existing RL algorithms are mostly suitable for continuous or discrete action spaces, which cannot be directly applicable to MIOC problems.

Discretizing continuous variables into finite discrete values and applying discrete RL methods, such as Rainbow [11], is a straightforward approach to tackle MIOC problems. However, this approach becomes impractical for high-dimensional control problems as it necessitates a substantial number of discrete values to achieve accurate outcomes.

In recent years, a substantial amount of RL research has focused on a special type of MIOC problems called parameterized action Markov decision process (PAMDP) [12]. The key of PAMDP is to formulate the problem as a hierarchical structure where each discrete action is associated with a set of continuous parameters. One approach is to alternate between optimizing the discrete action selection with Q-learning and the parameter selection with a policy search method [12]. Another approach called parameterized deep deterministic policy gradient (PA-DDPG) is to directly output the continuous parameters and weights for discrete actions from DDPG [13] and select the discrete action with the highest weight [14]. Parameterized deep Q-networks (P-DQN) combine the actor-critic architecture and DQN, where the actor network first outputs parameters for all discrete actions, and then the Q-network selects the action with the highest Q-value [15]. Other approaches utilize neural ordinary differential equations as state-value networks [16] or conditional variational auto-encoders [17] to handle the parameterized action space. Alternatively, some methods handle the mixed-integer action space in a unified manner. These approaches add extra layers [18] or parallel networks [19] to generate continuous and discrete actions, and then optimize the policy using techniques such as dueling DQN or proximal policy optimization.

In the domain of mixed-integer control for hybrid electric

This work was supported in part by Guangzhou Basic and Applied Basic Research Program under Grant 2023A04J1688, and in part by South China University of Technology faculty start-up fund. (*Corresponding author: Yuan Lin.*)

The authors are with the Shien-Ming Wu School of Intelligent Engineering at South China University of Technology, Guangzhou 511442, China (e-mail: wi_jinmingxu@mail.scut.edu.cn; yuanlin@scut.edu.cn).

vehicle (HEV) energy management, previous studies have employed various approaches, including utilizing frameworks similar to PA-DDPG [20] or P-DQN [21]. Tang *et al.* [22] combined DQN and DDPG, obtaining the gear ratio and engine throttle independently. However, no studies used RL to concurrently tackle the optimization of gear shifting and engine on/off control, which represents an unexplored research area in this field.

Inspired by the aforementioned research, this brief proposes a novel continuous-discrete reinforcement learning (CDRL) algorithm called twin delayed deep deterministic actor-Q (TD3AQ) for MIOC problems. The algorithm is applied to address an energy management problem for a plug-in hybrid electric vehicle (PHEV), aiming to demonstrate its effectiveness. The main contributions of this study are summarized as follows:

- 1) A state-of-the-art CDRL algorithm, TD3AQ, is proposed to address the mixed-integer action space. TD3AQ combines the advantages of both actor-critic and Q-learning methods, providing a unified solution for MIOC problems. Comparative evaluations demonstrate that TD3AQ achieves near-optimal solutions compared to dynamic programming (DP) and outperforms previous baselines [11], [14], [23]. Moreover, the sub-millisecond computation time of TD3AQ renders it suitable for real-time control applications.
- 2) This work pioneers the simultaneous optimization of two discrete variables, gear shift and clutch engagement/disengagement, using reinforcement learning for PHEV energy management. In contrast to previous studies [22] that rely on rule-based methods, this research emphasizes the systematic optimization [24] of gear shift and clutch engagement/disengagement for further fuel consumption reduction. The proposed approach is expected to yield superior energy management performance.

II. CONTINUOUS-DISCRETE REINFORCEMENT LEARNING

A. Reinforcement Learning

Reinforcement learning is a learning approach for optimal control by interacting with the environment. The objective is to develop an agent that can learn to make optimal decisions by maximizing a cumulative reward signal. Typically, this problem is formulated as a Markov decision process (MDP), which consists of a state space \mathcal{S} , an action space \mathcal{A} , an initial state distribution p_0 , and a transition probability $p(s', r|s, a)$ that specifies the probability of transitioning to state s' and receiving reward r when taking action a in state s , where $r(s, a) \in \mathbb{R}$. The agent's goal is to maximize the expected cumulative reward $\mathbb{E}[\sum_{t=0}^{\infty} \gamma^t r_t]$, where $\gamma \in [0, 1]$ is the discount factor.

According to the Bellman optimality principle, the value of a state under an optimal policy is the maximum expected return achievable from that state. Reinforcement learning algorithms gradually refine value function estimates and converge to the optimal policy, which maximizes cumulative reward.

To achieve this goal, there are two mainstream algorithms: value-based methods and policy-based methods. Value-based

methods learn the value function $V(s)$ or the action-value function $Q(s, a)$, which represent the expected cumulative reward starting from state s or taking action a in state s , respectively. The optimal policy $\pi^*(s)$ can be derived from the value function $V(s)$ or the action-value function $Q(s, a)$ by selecting the action that maximizes $Q(s, a)$, i.e., $\pi^*(s) = \arg \max_a Q(s, a)$. Policy-based methods, on the other hand, learn the parameterized policy $\pi_\theta(s)$ that can select actions without consulting a value function. The policy is updated by gradient ascent on a performance measure $J(\theta)$, where θ represents the parameters of the policy network. The policy network is a function approximator that maps the state s to the action a .

Actor-critic methods combine value-based and policy-based approaches. They learn both an approximate value function and a parameterized policy simultaneously, enabling efficient learning in complex environments.

B. Mixed-Integer Action Space

In this study, we explore the mixed-integer action space from the perspective of a parallel architecture, where discrete and continuous actions are independent of each other. For instance, in a PHEV energy management problem, the gear shift command could be the discrete action, while the engine torque could be the continuous action. These actions can be executed simultaneously and separately. Such mixed-integer action spaces can be defined as follows:

$$\mathcal{A} = \{a = (a^d, a^c) \mid a^d \in \mathcal{A}_d, a^c \in \mathcal{A}_c\} \quad (1)$$

where $\mathcal{A}_d \subseteq \mathbb{N}^m$ represents a finite set of discrete action spaces, $\mathcal{A}_c \subseteq \mathbb{R}^n$ denotes a continuous action space, and a^d and a^c are the discrete and continuous actions, respectively. The dimensionality of the action space is determined by $m+n$. To handle the action space for multi-dimensional discrete variables, a composite action vector can be employed. This vector has a length of $d_1 \times d_2 \times \dots \times d_m$, where d_i represents the number of discrete actions for the i -th dimension. Each element of the vector corresponds to a distinct combination of discrete actions.

C. TD3AQ Algorithm

To address the above mixed-integer action space, we propose a novel model-free algorithm, TD3AQ, which is based on the actor-critic framework. The forward propagation process of TD3AQ is shown in Fig. 1. The actor network μ_θ is used to generate the continuous actions a^c , then a^c and state s are fed into the Q-network to obtain the Q-values Q_1, Q_2, \dots, Q_k for each discrete action. Finally, the discrete action with the highest Q-value is selected as a^d . The details of the TD3AQ algorithm are elaborated below.

1) *Deep Deterministic Actor-Q*: Considering the vanilla DDPG algorithm [13], the Bellman equation is given by

$$Q_\omega(s, a) = \mathbb{E}_{r, s'} [r + \gamma Q_\omega(s', \mu_\theta(s'))] \quad (2)$$

where ω represents the parameters of the Q-network, μ_θ represents the actor network that approximates the optimal

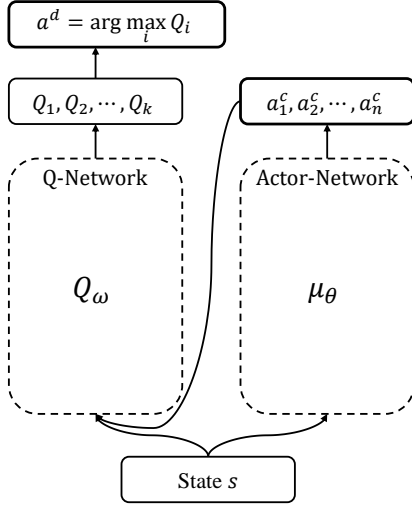


Fig. 1. The forward propagation process of TD3AQ. The continuous action a^c is generated by the actor network μ_θ , the subscript of a^c represents the dimension of the action space, and the discrete action a^d is selected by arg max operation on the Q-values.

action in the next state s' , and γ is the discount factor. The loss function to satisfy the Bellman equation is defined as

$$L(\omega) = \mathbb{E}_{(s,a,r,s') \sim \mathcal{B}} \left[(y - Q_\omega(s, a))^2 \right] \quad (3)$$

where \mathcal{B} is the replay buffer, a minibatch is sampled from \mathcal{B} to update the Q-network, y is the target value, which is defined as

$$y = r + \gamma Q_{\omega'}(s', \mu_{\theta'}(s')) \quad (4)$$

where ω' and θ' are the target networks to stabilize the training process. It is worth noting that the Eq. (2) holds only when the actor network μ_θ can provide the action that maximizes $Q_\omega(s, a)$. Assuming Q_ω is differentiable with respect to a , the actor network can be updated using the gradient ascent method by maximizing

$$J(\theta) = \mathbb{E}_{s \sim \mathcal{B}} [Q_\omega(s, \mu_\theta(s))] \quad (5)$$

Note that the parameters of Q_ω are fixed during the actor network update.

Deep deterministic actor-Q (DDAQ) [25] adopts the same architecture as DDPG, but instead of approximating a single Q-value, it approximates k Q-values for the k discrete actions. Therefore, the Bellman equation can be rewritten as

$$Q_\omega(s, a) = \mathbb{E}_{r,s'} \left[r + \gamma \max_{a^d \in \mathcal{A}_d} Q_\omega(s', a^d, \mu_\theta(s')) \right] \quad (6)$$

Additionally, the loss function can be defined as

$$L(\omega) = \mathbb{E}_{(s,a,r,s') \sim \mathcal{B}} \left[(y - Q_\omega(s, a^d, a^c))^2 \right] \quad (7)$$

where

$$y = r + \gamma \max_{a^d \in \mathcal{A}_d} Q_{\omega'}(s', a^d, \mu_{\theta'}(s')) \quad (8)$$

When updating the actor network, since the discrete action with the highest Q-value is selected as the output, the objective function is defined as

$$J(\theta) = \mathbb{E}_{s \sim \mathcal{B}} \left[\max_{a^d \in \mathcal{A}_d} Q(s, a^d, \mu_\theta(s)) \right] \quad (9)$$

where the maximum Q-value is used as the objective function. In previous work (P-DQN) [15], the objective function was defined as the sum of all Q-values, which posed a problem when back propagating gradients: updating the weights in the Q-network during back propagation affected all weights in the network, including those unrelated to the action with the highest Q-value, potentially causing the algorithm to update in an incorrect direction. DDAQ addresses this issue by using the maximum Q-value as the objective function, ensuring that only the weights corresponding to the action a^d with the highest Q-value are updated.

2) *TD3AQ*: DDPG has shown potential in achieving good performance, but its robustness is limited due to its sensitivity to hyperparameters. This is mainly because DDPG tends to overestimate Q-values, which results in poor policy updates. To address this issue, we combine DDAQ and TD3 [26] to form TD3AQ. Three key modifications to improve the performance are introduced.

a) *Target policy smoothing*: a noise sampled from a normal distribution is added to the action generated by the target actor network. This technique acts as a regularizer that prevents the actor network from converging to a suboptimal solution. Specifically, the action was smoothed by adding a clipped noise, defined as follows:

$$\tilde{a}^c = \text{clip}(\mu_{\theta'}(s') + \text{noise}, a_{min}^c, a_{max}^c) \quad (10)$$

where a_{min}^c and a_{max}^c are the lower and upper bounds of the continuous action, respectively. The *noise* is defined as:

$$\text{noise} = \text{clip}(\epsilon, \epsilon_l, \epsilon_h), \quad \epsilon \sim \mathcal{N}(0, \sigma^2) \quad (11)$$

where ϵ_l and ϵ_h are the lower and upper bounds of the noise ϵ , respectively. The noise ϵ is sampled from a normal distribution with mean 0 and standard deviation σ .

b) *Clipped double Q-learning*: to mitigate the overestimation of Q-values, a twin Q-network is introduced to DDAQ. When updating the Q-network, the minimum of the two selected Q-values is used as the target value:

$$y = r + \gamma \min_{j=1,2} \left(\max_{a^d \in \mathcal{A}_d} Q_{\omega_j'}(s', a^d, \tilde{a}^c) \right) \quad (12)$$

then both Q-networks are updated by minimizing the mean squared error between the target value and the Q-value:

$$L(\omega_j) = \mathbb{E}_{(s,a,r,s') \sim \mathcal{B}} \left[(y - Q_{\omega_j}(s, a^d, a^c))^2 \right], \quad j = 1, 2 \quad (13)$$

c) *Delayed updates*: the actor network and target networks are updated less frequently than the Q-networks. This helps to stabilize the training process since slowing down the actor allows the critic to learn more accurate Q-values before letting it guide the actor. The networks are updated every two iterations as recommended in [26].

The proposed TD3AQ pseudo-code is shown in Algorithm 1, with all the proposed improvements combined.

III. PHEV ENERGY MANAGEMENT PROBLEM FORMULATION

To validate the proposed TD3AQ algorithm, this work considers a PHEV energy management problem, which presents a

Algorithm 1: Pseudo-code of the TD3AQ Algorithm

Input: Gradient stepsizes $\{\alpha, \beta, \rho\} \geq 0$, exploration noise $\eta = \mathcal{N}(0, \delta^2)$, exploration parameter ε , minibatch size B , empty replay buffer \mathcal{B} , target smooth noise $\epsilon \sim \mathcal{N}(0, \sigma^2)$, target smooth noise bounds ϵ_l, ϵ_h , discount factor γ , policy update frequency K .

- 1 Initialize Q-network $Q_{\omega_1}, Q_{\omega_2}$, and actor network μ_θ with random weights $\omega_1, \omega_2, \theta$;
 - 2 Initialize target networks $\omega'_1 \leftarrow \omega_1, \omega'_2 \leftarrow \omega_2, \theta' \leftarrow \theta$;
 - 3 Initialize replay buffer \mathcal{B} ;
 - 4 **for** $t = 1, 2, \dots, T$ **do**
 - 5 Clear local gradients $d\omega_1 \leftarrow 0, d\omega_2 \leftarrow 0, d\theta \leftarrow 0$;
 - 6 Compute continuous action with exploration noise $a_t^c = \text{clip}(\mu_\theta(s_t) + \eta, a_{min}^c, a_{max}^c)$;
 - 7 Compute discrete action a_t^d according to ε -greedy

$$\begin{cases} \Pr(a_t^d = \text{a sample randomly from } \mathcal{A}_d) = \varepsilon, \\ \Pr(a_t^d = \arg \max_{a^d} Q_{\omega_1}(s_t, a^d, a_t^c)) = 1 - \varepsilon \end{cases}$$
 - 8 Take action $a_t = (a_t^d, a_t^c)$, observe reward r_t and the next state s_{t+1} ;
 - 9 Store transition (s_t, a_t, r_t, s_{t+1}) in replay buffer \mathcal{B} ;
 - 10 Sample B transitions $\{(s_i, a_i, r_i, s_{i+1})\}_{i \in [B]}$ from \mathcal{B} ;
 - 11 Compute target continuous action $\tilde{a}_i^c = \text{clip}(\mu_{\theta'}(s_{i+1}) + \text{clip}(\epsilon, \epsilon_l, \epsilon_h), a_{min}^c, a_{max}^c)$
 - 12 Compute the target value
$$y_i = r_i + \gamma \min_{j=1,2} \left(\max_{a^d \in \mathcal{A}_d} Q_{\omega'_j}(s_{i+1}, a^d, \tilde{a}_i^c) \right)$$
 - 13 Update the two Q-networks ($j = 1, 2$) by one step of gradient descent
$$\omega_j \leftarrow \omega_j - \alpha \nabla_{\omega_j} \frac{1}{|B|} \sum_{i \in [B]} (Q_{\omega_j}(s_i, a_i^d, a_i^c) - y_i)^2$$
 - 14 **if** $t \bmod K == 0$ **then**
 - 15 Update the actor network by one step of gradient ascent
$$\theta \leftarrow \theta + \beta \nabla_{\theta} \frac{1}{|B|} \sum_{i \in [B]} \max_{a^d} Q_{\omega_1}(s_i, a^d, \mu_\theta)$$
 - 16 Update the target networks ($j = 1, 2$) with
$$\omega'_j \leftarrow \rho \omega_j + (1 - \rho) \omega'_j, \quad \theta' \leftarrow \rho \theta + (1 - \rho) \theta'$$
 - 17 **end**
 - 18 **end**
-

challenging MIOC problem as it requires simultaneous control of continuous power distribution and discrete gear selection for a highly non-linear hybrid system. The section begins with an introduction to the PHEV powertrain modeling, followed by the MIOC problem formulation.

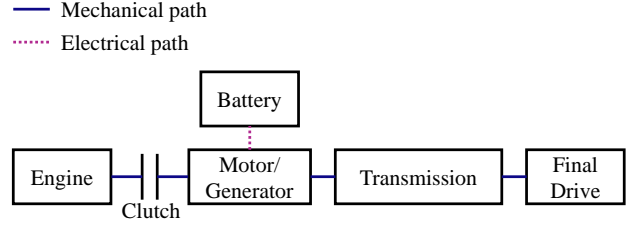


Fig. 2. The parallel hybrid powertrain architecture.

A. PHEV Powertrain Configuration

This study focuses on a parallel hybrid electric vehicle [27]. The powertrain architecture comprises an internal combustion engine, an electric motor, a clutch, and an automated manual transmission, as depicted in Fig. 2. The vehicle's HEV mode can be altered by engaging or disengaging the clutch between the engine and the motor, providing three modes of operation: motor-only, engine-only, and hybrid-drive.

B. Vehicle Dynamics

The vehicle dynamics are described by the following equations:

$$T_w = \left[ma + \frac{1}{2} C_d \rho A v^2 + \mu mg \cos \theta + mg \sin \theta \right] r \quad (14)$$

$$\omega = \frac{v}{r} i_d i_g \quad (15)$$

where T_w is the wheel torque, m is the vehicle mass, a is the vehicle acceleration, C_d is the air drag coefficient, ρ is the air density, A is the vehicle cross section area, ω is the shaft angular velocity, v is the vehicle velocity, μ is the rolling resistance coefficient, g is the gravitational acceleration, θ is the road grade, r is the tyre radius, i_d is the final drive gear ratio, and i_g is the transmission gear ratio.

The torque on the wheel can be denoted as:

$$T_w = (cT_{e,d} + T_m) i_d i_g \eta_d \eta_g - T_b \quad (16)$$

where $T_{e,d}$ and T_m represent the driving torque transmitted from the engine and motor to the shaft, respectively. c is the clutch state with $c = 1$ representing the clutch engaged and $c = 0$ representing the clutch disengaged. η_d is the final drive efficiency, η_g is the transmission efficiency, and T_b is the mechanical brake torque.

C. Engine Model

The engine torque is separated into two parts: the driving torque $T_{e,d}$ and the idle torque $T_{e,i}$, which can be expressed as:

$$T_e = T_{e,d} + T_{e,i} \quad (17)$$

$$\text{s.t. } 0 \leq T_e \leq T_{e,max} \quad (18)$$

where $T_{e,max} = f_e(\omega_e)$ represents the maximum engine torque at a given angular velocity ω_e , which is depicted in Fig. 3. When the clutch is disengaged, $T_{e,d}$ is set to zero, and $T_e = T_{e,i}$. The idle torque primarily serves to power

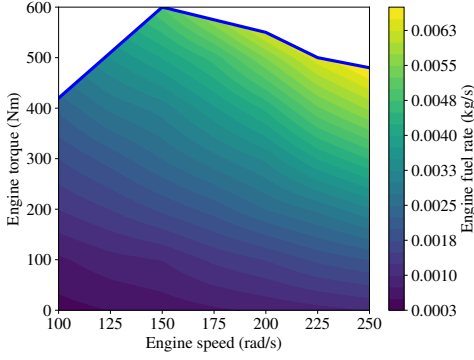


Fig. 3. The engine fuel rate map, where the boundary represents the maximum engine torque.

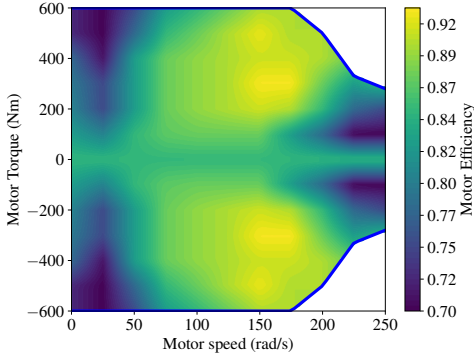


Fig. 4. The motor efficiency map, where the upper and lower boundaries represent the maximum and minimum motor torque, respectively.

the auxiliary systems. The engine speed is governed by the following equation:

$$\omega_e = \begin{cases} \omega, & \text{if } c = 1 \\ \omega_{ei}, & \text{if } c = 0 \end{cases} \quad (19)$$

$$\text{s.t. } \omega_e \geq \omega_{ei}, \quad \text{if } c = 1 \quad (20)$$

where ω_m is the motor angular velocity, and ω_{ei} is the engine idle angular velocity. The constraint on ω_e is imposed to ensure that the engine speed does not drop below the idle speed when the clutch is engaged.

The fuel rate can then be described by:

$$\dot{m}_f = f_f(\omega_e, T_e) \quad (21)$$

where \dot{m}_f is the fuel rate (kg/s), and f_f is the fuel rate interpolation function, which is shown in Fig. 3.

D. Motor Model

The motor torque T_m is governed by the following constraints:

$$-f_m(\omega) = T_{m,min} \leq T_m \leq T_{m,max} = f_m(\omega) \quad (22)$$

where $T_{m,max}$ and $T_{m,min}$ are the maximum and minimum motor torque at a given angular velocity, respectively. f_m is an interpolation function that is used to calculate $T_{m,max}$ and $T_{m,min}$, which is depicted in Fig. 4.

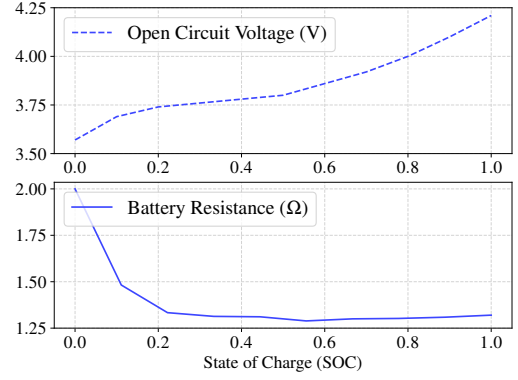


Fig. 5. The open-circuit voltage and resistance of the battery cell.

E. Battery Model

We consider a lithium-ion battery pack consisting of 112 cells, where the cells are connected in series. The battery model is based on the battery state of charge (SOC) and the battery open-circuit voltage E . The battery SOC is calculated by:

$$\dot{SOC} = -\frac{E - \sqrt{E^2 - 4R_b P_b}}{2R_b Q_{max}} \quad (23)$$

$$P_b = T_m \omega \eta_m^{\text{sgn}(-T_m)} \quad (24)$$

$$\eta_m = f_\eta(\omega, T_m) \quad (25)$$

where I_b is the net current, Q_{max} is the battery capacity, R_b is the battery resistance, P_b is the battery power, η_m is the motor efficiency, and f_η is the motor efficiency interpolation function, which is shown in Fig. 4. The battery open-circuit voltage and resistance are denoted as functions of the battery SOC, as illustrated in Fig. 5.

F. Problem Formulation

The primary objective of the PHEV energy management system is to develop a control strategy that minimizes the equivalent cost of fuel and electricity consumption, while simultaneously reducing the frequency of gear shifts and clutch engagement to enhance the overall driving experience. The control inputs to the system are the engine torque, mechanical brake torque, gear ratio, and clutch state:

$$u = [T_e, T_b, \varsigma, c]^T \quad (26)$$

assuming that only a sequential shift pattern is considered, ς belongs to the set $\{-1, 0, 1\}$, where $\varsigma = -1$ represents downshift, $\varsigma = 1$ represents upshift, and $\varsigma = 0$ corresponds to sustainment. The cost function to minimize can be expressed as:

$$J = \sum_{T_0}^{T_{cyc}} (k_f \dot{m}_f + k_b P_b + p_\varsigma + p_c) \Delta t \quad (27)$$

$$p_\varsigma = \zeta \cdot \tilde{p}, \quad \text{if } |gear_t - gear_{t-1}| > 0 \quad (28)$$

$$p_c = \xi \cdot \tilde{p}, \quad \text{if } |c_t - c_{t-1}| > 0 \quad (29)$$

where k_f and k_b are the fuel and electricity prices, respectively, \tilde{p} is the reference penalty, which is set to be the

intermediate value of fuel consumption, p_ζ and p_c are the penalties for gear shift and clutch engagement/disengagement, respectively, ζ and ξ are the penalty coefficients, Δt is the control interval, T_0 and T_{cyc} are the initial and final time steps of the drive cycle, respectively. The drive cycle utilized for training is the China heavy-duty transient cycle for light trucks (CHTC-LT).

IV. EXPERIMENTS AND DISCUSSION

A. TD3AQ for PHEV Energy Management

1) *State*: The observation space of the RL agent is defined as the state of the system, which is a vector of the following variables:

$$s = [v, a, T_w, SOC, i_g, c] \quad (30)$$

2) *Action*: The action space is defined by the torque relationship in Eq. (18) as follows:

$$a = [T_e, \varsigma, c] \quad (31)$$

where T_e is continuous, and ς and c are discrete, making it an MIOC problem. In negative demand torque, regenerative braking is prioritized for battery charging. If regenerative braking is insufficient, mechanical braking provides the remaining torque. In positive demand torque, the mechanical braking torque is set to zero, and the engine and motor supply the demand torque. Thus, the proposed action determines the vehicle's torque distribution entirely.

To handle the multi-discrete action space involving two actions, ς and c , we employ a composite action vector. This vector, with a length of $3 \times 2 = 6$, represents specific combinations of three gear shift actions and two clutch actions. This approach effectively manages the multi-discrete action space while maintaining a compact representation.

3) *Reward*: In addition to the cost function defined in Eq. (27), it is imperative to ensure that the system dynamics remain within specific constraints. Thus, the reward function is designed as a combination of fuel consumption and the penalty for violating the constraints. The detailed hand-crafted reward function is defined as follows:

$$r = r_{cost} - p_\omega - p_{T_m} - p_{SOC} \quad (32)$$

$$r_{cost} = -(k_f \dot{m}_f + k_b P_b + p_\zeta + p_c) \quad (33)$$

$$p_\omega = \tilde{p}, \quad \text{if } \omega > \omega_{max} \quad (34)$$

$$p_{T_m} = 10\tilde{p}, \quad \text{if } T_m > T_{m,max} \quad (35)$$

$$p_{SOC} = \begin{cases} 0, & \text{if } SOC_l \leq SOC \leq SOC_h \\ 10\tilde{p} \cdot \frac{|SOC - SOC_h|}{1 - SOC_h}, & \text{if } SOC > SOC_h \\ 10\tilde{p} \cdot \frac{|SOC - SOC_l|}{SOC_l}, & \text{if } SOC < SOC_l \end{cases} \quad (36)$$

where p_ω , p_{T_m} , and p_{SOC} are the penalties for exceeding the constraints on the motor torque, shaft angular velocity, and SOC, respectively. The penalty for exceeding the SOC constraint is designed as a linear function of the SOC deviation from the desired range, which extends from the lower bound SOC_l to the upper bound SOC_h . Therefore, the greater the deviation of the SOC from the desired range, the higher the penalty.

TABLE I
SIMULATION RESULTS FOR CHTC-LT

Strategy	τ_{sh}	τ_{cl}	ν_{T_m}	ν_ω	ν_{soc}	Cost/¥	Gap
DP	52	32	-	-	-	15.04	-
TD3AQ	116	56	0	0	0	15.66	4.13%
DDAQ	87	48	0	0	0	16.21	7.80%
PATD3	226	174	1	5	0	16.58	10.21%
Rainbow	251	208	0	1	0	16.22	7.85%

B. Comparison Benchmarks

Four benchmark methods, DP, DDAQ [25], PATD3 [14], and Rainbow [11], are selected for comparison. DP employs the MATLAB toolbox developed by Sundström *et al.* [28]. The continuous engine torque is discretized with an interval of 25 Nm. Empirical experiments have demonstrated that finer discretization does not improve the performance significantly (less than 0.05% improvement in cost with 10 Nm discretization while requiring seven times more computation time). Since Rainbow is designed for discrete action spaces, it adopts the same discretization scheme as DP. All RL algorithms utilize Optuna [29] to tune the hyperparameters.

C. Experimental Setup

The training process involves a total of 200 000 timesteps, where each timestep represents one second of driving time. Model evaluation was performed every 10 000 timesteps, with each evaluation period lasting one episode, i.e., one drive cycle. The final model for testing was selected based on the highest return achieved during evaluation. All experiments were conducted on a desktop computer equipped with an AMD Ryzen 9 5950X CPU and an NVIDIA GeForce RTX 3080 Ti GPU. The source code of the algorithm is available at <https://github.com/xujinming01/TD3AQ>.

D. Optimal Control Performance

Fig. 6 displays the hybrid action output of DP and TD3AQ employed in CHTC-LT. It is evident that TD3AQ exhibits similar output trends to DP, however, with a higher frequency of gear shifts and clutch state changes. Notably, DP operates under the assumption that the entire drive cycle is known in advance. In contrast, RL algorithms only possess access to the current state, yielding suboptimal solutions. Table I presents the simulation results for CHTC-LT, where τ_{sh} and τ_{cl} denote the number of gear shifts and clutch engagements, respectively, ν_{T_m} , ν_ω , and ν_{soc} denote the instances where motor torque, shaft angular velocity, and SOC exceed the predefined constraints. Among the RL algorithms, TD3AQ exhibits the lowest cost, with a gap of 4.13% compared to DP. Furthermore, TD3AQ and DDAQ do not violate any constraints, while PATD3 and Rainbow demonstrate a few violations in terms of motor torque and shaft angular velocity constraints.

Fig. 7 depicts the SOC trajectories for the RL algorithms and DP. It is observed that the RL algorithms generally exhibit similar SOC trajectories to DP, except during the final portions of the drive cycle. Given that the lower bound SOC_l is

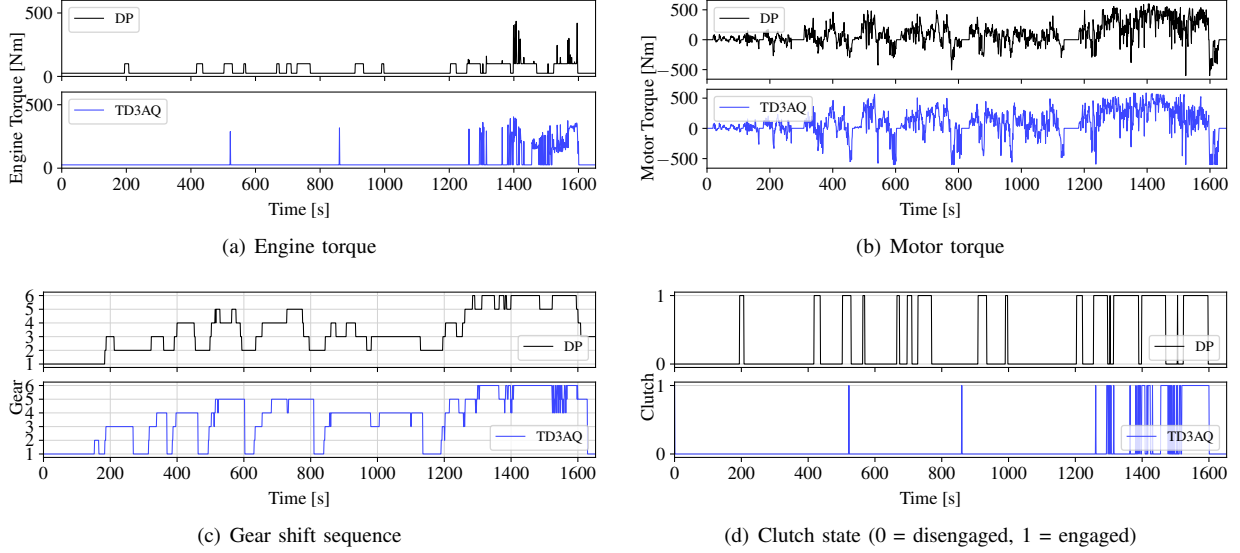


Fig. 6. The hybrid action output of DP and TD3AQ for CHTC-LT.

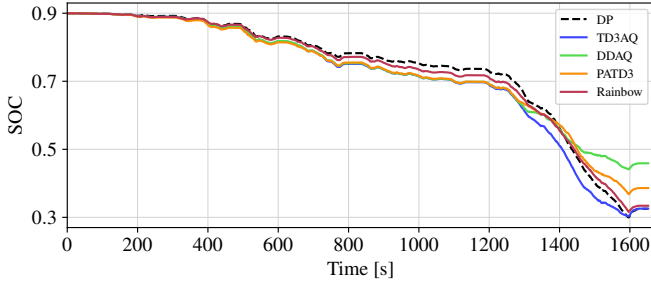


Fig. 7. SOC trajectories of CHTC-LT drive cycle.

TABLE II
WALL-CLOCK TIME COMPARISON FOR CHTC-LT

Strategy	Training time (h)	step time (ms)
TD3AQ	0.18	0.38
DDAQ	0.17	0.36
PATD3	0.18	0.74
Rainbow	0.59	0.97
DP	N/A	96599

set to 0.3, all the algorithms reach an SOC of 0.3 by the end of the drive cycle, with the exception of DDAQ and PATD3. Importantly, it is worth emphasizing that there are no violations of the SOC constraint, indicating that RL algorithms can effectively learn to regulate the SOC within the desired range without prior knowledge of the specific drive cycle.

Table II presents the time consumption comparison for CHTC-LT, where *step time* represents the time required to execute a single action during testing. While DP can obtain the optimal solution for each step in a single calculation, it comes at the expense of a significant amount of time, with its single solution time being six orders of magnitude greater than RL. This substantial discrepancy in time consumption highlights the efficiency of the RL algorithms, as indicated by their step times falling within the millisecond range. Consequently, RL

TABLE III
GENERALIZATION RESULTS OF THE NEW CYCLES

Test cycle	Strategy	ν_{T_m}	ν_{ω}	ν_{soc}	Cost/¥	Gap
JE05	DP	-	-	-	13.60	-
	TD3AQ	1	0	0	14.04	3.23%
	DDAQ	0	0	0	14.61	7.41%
	PATD3	6	2	0	14.77	8.60%
	Rainbow	0	0	0	14.76	8.48%
HD-UDDS	DP	-	-	-	9.27	-
	TD3AQ	4	0	0	9.88	5.94%
	DDAQ	0	8	0	10.55	13.18%
	PATD3	14	7	0	9.97	6.95%
	Rainbow	10	7	0	10.38	11.36%
WHVC	DP	-	-	-	5.51	-
	TD3AQ	0	0	0	5.72	3.63%
	DDAQ	0	0	0	5.89	6.78%
	PATD3	0	1	0	5.80	5.16%
	Rainbow	1	0	0	6.13	10.99%

demonstrates promising potential for real-time optimal control applications.

E. Generalization Results

To evaluate the generalization capabilities of the proposed CDRL algorithm TD3AQ, the model trained exclusively on the CHTC-LT drive cycle is tested on three additional drive cycles: JE05, HD-UDDS, and WHVC. The simulation results are summarized in Table III.

The findings demonstrate that the TD3AQ algorithm exhibits commendable generalization performance when applied to new drive cycles. In comparison with other RL algorithms, TD3AQ closely approximates the cost achieved by the DP strategy, with an average gap of 4.27% across the three cycles. However, the remaining RL algorithms display a larger deviation in terms of cost.

Furthermore, it is worth noting that all RL algorithms exhibit a higher frequency of constraint violations in the new

drive cycles, particularly PATD3 and Rainbow. This issue primarily arises from the inherent limitation of RL in enforcing hard constraints during the training process.

V. CONCLUSION

In this brief, we present a novel reinforcement learning algorithm called TD3AQ for solving mixed-integer optimal control problems. The TD3AQ algorithm uses actor-Q networks to directly generate continuous and discrete actions from the current state. We evaluate the proposed TD3AQ algorithm on a hybrid electric vehicle energy management problem and show that it achieves satisfactory performance with a cost gap of 4.13% compared to the DP strategy. TD3AQ's ability to generalize is demonstrated through the results on three new drive cycles. The algorithm's sub-millisecond response time indicates its significant potential for real-time, mixed-integer optimal control applications. However, note that the algorithm carries the risk of violating constraints, which, if unaddressed, could potentially lead to vehicle and battery damage in real-world scenarios. Future work will focus on extending TD3AQ to more complex, higher-dimensional problems to further substantiate its adaptability and robustness, and developing CDRL algorithms with safety guarantees.

REFERENCES

- [1] A. Kasis, S. Timotheou, and M. Polycarpou, "Optimal secondary frequency regulation with on-off loads in power networks," *IEEE Transactions on Control Systems Technology*, vol. 30, no. 6, pp. 2490–2505, 2022.
- [2] D. Corona and B. De Schutter, "Adaptive cruise control for a SMART car: A comparison benchmark for MPC-PWA control methods," *IEEE Transactions on Control Systems Technology*, vol. 16, no. 2, pp. 365–372, 2008.
- [3] Y. Shao and Z. Sun, "Vehicle speed and gear position co-optimization for energy-efficient connected and autonomous vehicles," *IEEE Transactions on Control Systems Technology*, vol. 29, no. 4, pp. 1721–1732, 2020.
- [4] D. R. Morrison, S. H. Jacobson, J. J. Sauppe, and E. C. Sewell, "Branch-and-bound algorithms: A survey of recent advances in searching, branching, and pruning," *Discrete Optimization*, vol. 19, pp. 79–102, 2016.
- [5] R. E. Bellman, *Dynamic programming*. Princeton university press, 2010.
- [6] M. Fischetti and A. Lodi, "Heuristics in mixed integer programming," *Wiley Encyclopedia of Operations Research and Management Science*, 2010.
- [7] P. Belotti, C. Kirches, S. Leyffer, J. Linderoth, J. Luedtke, and A. Mahajan, "Mixed-integer nonlinear optimization," *Acta Numerica*, vol. 22, pp. 1–131, 2013.
- [8] O. Vinyals, I. Babuschkin, W. M. Czarnecki, M. Mathieu, A. Dudzik, J. Chung, D. H. Choi, R. Powell, T. Ewalds, P. Georgiev *et al.*, "Grandmaster level in StarCraft II using multi-agent reinforcement learning," *Nature*, vol. 575, no. 7782, pp. 350–354, 2019.
- [9] E. Kaufmann, L. Bauersfeld, A. Loquercio, M. Müller, V. Koltun, and D. Scaramuzza, "Champion-level drone racing using deep reinforcement learning," *Nature*, vol. 620, no. 7976, pp. 982–987, 2023.
- [10] R. S. Sutton and A. G. Barto, *Reinforcement learning: An introduction*. MIT press, 2018.
- [11] M. Hessel, J. Modayil, H. Van Hasselt, T. Schaul, G. Ostrovski, W. Dabney, D. Horgan, B. Piot, M. Azar, and D. Silver, "Rainbow: Combining improvements in deep reinforcement learning," in *AAAI Conference on Artificial Intelligence (AAAI)*, vol. 32, no. 1, 2018, pp. 3215–3222.
- [12] W. Masson, P. Ranchod, and G. Konidaris, "Reinforcement learning with parameterized actions," in *AAAI Conference on Artificial Intelligence (AAAI)*, vol. 30, no. 1, 2016, pp. 1934–1940.
- [13] T. P. Lillicrap, J. J. Hunt, A. Pritzel, N. Heess, T. Erez, Y. Tassa, D. Silver, and D. Wierstra, "Continuous control with deep reinforcement learning," in *International Conference on Learning Representations (ICLR)*, 2016.
- [14] M. Hausknecht and P. Stone, "Deep reinforcement learning in parameterized action space," in *International Conference on Learning Representations (ICLR)*, 2016.
- [15] J. Xiong, Q. Wang, Z. Yang, P. Sun, L. Han, Y. Zheng, H. Fu, T. Zhang, J. Liu, and H. Liu, "Parameterized deep Q-networks learning: Reinforcement learning with discrete-continuous hybrid action space," *arXiv preprint arXiv:1810.06394*, 2018.
- [16] S. Massaroli, M. Poli, S. Bakhtiyarov, A. Yamashita, H. Asama, and J. Park, "Neural ordinary differential equation value networks for parameterized action spaces," in *ICLR 2020 Workshop on Integration of Deep Neural Models and Differential Equations*, 2020.
- [17] B. Li, H. Tang, Y. Zheng, J. Hao, P. Li, Z. Wang, Z. Meng, and L. Wang, "HyAR: Addressing discrete-continuous action reinforcement learning via hybrid action representation," in *International Conference on Learning Representations (ICLR)*, 2022.
- [18] X. Jiang and Y. Ji, "HD3: Distributed dueling DQN with discrete-continuous hybrid action spaces for live video streaming," in *ACM International Conference on Multimedia (ACM MM)*, 2019, pp. 2632–2636.
- [19] Z. Fan, R. Su, W. Zhang, and Y. Yu, "Hybrid actor-critic reinforcement learning in parameterized action space," in *International Joint Conference on Artificial Intelligence (IJCAI)*, 2019, pp. 2279–2285.
- [20] Y. Li, H. He, A. Khajepour, H. Wang, and J. Peng, "Energy management for a power-split hybrid electric bus via deep reinforcement learning with terrain information," *Applied Energy*, vol. 255, p. 113762, 2019.
- [21] H. Wang, H. He, Y. Bai, and H. Yue, "Parameterized deep Q-network based energy management with balanced energy economy and battery life for hybrid electric vehicles," *Applied Energy*, vol. 320, p. 119270, 2022.
- [22] X. Tang, J. Chen, H. Pu, T. Liu, and A. Khajepour, "Double deep reinforcement learning-based energy management for a parallel hybrid electric vehicle with engine start-stop strategy," *IEEE Transactions on Transportation Electrification*, vol. 8, no. 1, pp. 1376–1388, 2021.
- [23] Y. Ran, H. Hu, Y. Wen, and X. Zhou, "Optimizing energy efficiency for data center via parameterized deep reinforcement learning," *IEEE Transactions on Services Computing*, vol. 16, no. 2, pp. 1310–1323, 2022.
- [24] V. Ngo, T. Hofman, M. Steinbuch, and A. Serrarens, "Optimal control of the gearshift command for hybrid electric vehicles," *IEEE Transactions on Vehicular Technology*, vol. 61, no. 8, pp. 3531–3543, 2012.
- [25] J. Zhang, J. Du, Y. Shen, and J. Wang, "Dynamic computation offloading with energy harvesting devices: A hybrid-decision-based deep reinforcement learning approach," *IEEE Internet of Things Journal*, vol. 7, no. 10, pp. 9303–9317, 2020.
- [26] S. Fujimoto, H. Hoof, and D. Meger, "Addressing function approximation error in actor-critic methods," in *International Conference on Machine Learning (ICML)*. PMLR, 2018, pp. 1587–1596.
- [27] H. Yu, F. Zhang, J. Xi, and D. Cao, "Mixed-integer optimal design and energy management of hybrid electric vehicles with automated manual transmissions," *IEEE Transactions on Vehicular Technology*, vol. 69, no. 11, pp. 12 705–12 715, 2020.
- [28] O. Sundström and L. Guzzella, "A generic dynamic programming matlab function," in *IEEE control applications,(CCA) & intelligent control,(ISIC)*. IEEE, 2009, pp. 1625–1630.
- [29] T. Akiba, S. Sano, T. Yanase, T. Ohta, and M. Koyama, "Optuna: A next-generation hyperparameter optimization framework," in *ACM SIGKDD International Conference on Knowledge Discovery and Data Mining*, 2019, pp. 2623–2631.